Relativistic Quantum Mechanics (McGraw-Hill, New York, 1964), have been adopted in this paper.

[8]This appears to be what was finally done in Ref. 3, and the results obtained there should have agreed with those presented in this paper.

[9]P. Pascual and E. de Rafael, Lett. Nuovo Cimento 4, 1144 (1970).

[10]J. Aldins, S. J. Brodsky, A. J. Dufner, and T. Kinoshita, Phys. Rev. D 1, 2378 (1970).

[11]Note that changing the sign of $\Gamma_g{}'^s$ leads to agreement with Ref. 3 for this graph. To check for sign errors in our computer programs we used them to compute Γ_g without infrared subtractions. The results diverged linearly to $+\infty$ as would be expected from the $1/p$ term in $\Gamma_g{}'^{IR}$.

[12]A. C. Hearn, Stanford University Report No. ITP-247 (unpublished).

[13]This program is described by A. J. Dufner, in Proceedings of the Colloquium on Computational Methods in Theoretical Physics, Marseille, 1970 (unpublished).

[14]G. P. Lepage, SLAC Report No. SLAC-PUB-1839, 1976 (to be published).

Experimental Measurement of Electron Heat Diffusivity in a Tokamak*

J. D. Callen and G. L. Jahns
Oak Ridge National Laboratory, Oak Ridge, Tennessee 37830
(Received 14 October 1976)

Electron temperature perturbations produced by internal disruptions in the center of the Oak Ridge Tokamak (ORMAK) are followed with a multichord soft-x-ray detector array. The space-time evolution is found to be diffusive in character, but the conduction coefficient determined from a heat-pulse-propagation model is larger by a factor of 2.5–15 than that implied by the measured gross energy-containment time.

A useful model for understanding the energy transport governing the behavior of tokamak discharges is a three-region plasma model. The central-core region ($r < a_D$, the disruption radius) suffers internal disruptions[1] repeatedly as the safety factor q drops below unity. Outside this core region there is typically a large "middle" region (confinement zone) where tearing modes, plasma turbulence and/or unknown processes are responsible for "anomalous" heat transport, which primarily determines the energy containment of the device. Finally, there is a "plasma-edge" region ($r > a_0$) dominated by atomic physics effects such as radiation, impurity refluxing, charge exchange, etc.

The internal disruptions inside a_D manifest themselves as sudden drops in the soft-x-ray signal level, followed by slower recoveries, giving the characteristic sawtooth pattern evident in Fig. 1. The standard interpretation[1] of the sudden drop is that the electron temperature is decreasing as heat is rapidly lost from the central region. This process, which we will not discuss in detail, results in a pulse of heat into the volume just outside the disruption radius, and predictably, as seen in Fig. 1, the x-ray signals outside a_D show a pulselike increase at the time of the sudden decrease inside. By following the propagation of these perturbations through the critical middle region, we can, directly and for the first time, examine the fundamental electron-heat-transport process in tokamaks.

The soft-x-ray system on ORMAK consists of nine silicon diffused-junction diode detectors that view different fixed chords through the plasma.[2] The x-ray signal results from plasma bremsstrahlung and recombination processes, both of which are strongly dependent on tempera-

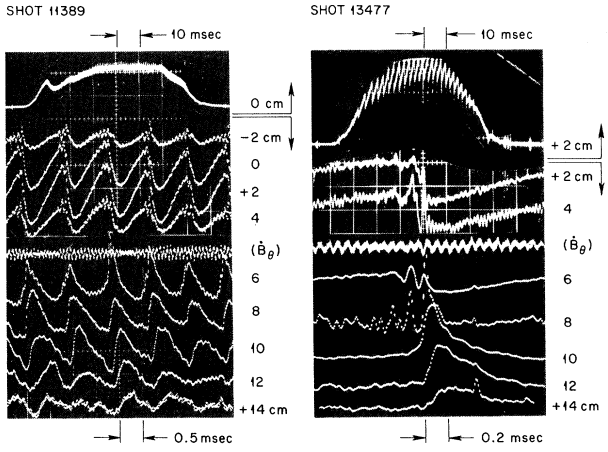

FIG. 1. Composite oscillograms of soft-x-ray signals for two discharges. For both cases, the top trace gives the signal from one detector over the full time of the discharge; the rest of the signals are on an expanded timescale starting at 45 msec, which falls in the middle of the full-time trace. Amplification factors are different for purposes of display. The temporal variation in the signal (sharp fall inside, sharp rise outside) shows that a_D is $\simeq 5$ cm for shot 11 389 and $\simeq 8$ cm for shot 13477. The signals labeled $\dot{B}_\theta$ are poloidal magnetic field fluctuations from pickup loops.

ture and density. Thus, most of the radiation seen by a given detector comes from the small volume where the temperature and density have their largest values along the viewing chord; hence this is more of a point measurement rather than an average one. The detectors are arranged so that these points lie 2 cm apart and are collimated so that their spatial resolution is about 1.7 cm. The output current of the detectors is proportional to the net radiation power in the 2 or 3 to 12 keV energy range, where the low-energy cutoff (E_c) is selected by choice of beryllium foil thickness.

Figure 1 shows two examples of the resulting x-ray signal on an expanded time scale that starts at 45 msec into the discharge, by which time steady-state conditions have been established. The principal features of the heat pulses for $r > a_D$ are that the times at which the pulses peak are progressively delayed, and that the pulses are broadened, as they move out from the center.

We hypothesize a theoretical model for the propagation process described above from an electron-heat-balance equation. In order to concentrate on the transport in the confinement zone, we assume we can ignore the effects of the internal disruption beyond some radius r, i.e., for $r \gtrsim a_D$. Keeping only heat conduction terms (justified below), the electron-heat-balance equation becomes

$$(\partial/\partial t)(\tfrac{3}{2}n_e T_e) = r^{-1}(\partial/\partial r)(r n_e \chi_{ep} \partial T_e/\partial r), \quad (1)$$

where χ_{ep} is the generalized electron-heat-conduction coefficient that governs the pulse evolution.

The observed temperature fluctuations are small (typically $\Delta T_e \leq 0.2 T_e$), so we solve a perturbation form of Eq. (1). Since the internal disruptions apparently have their primary effect on the electron temperature and have little effect on the density,[3] we assume $T_e \to T_e + \Delta T_e$ with n_e unchanged, and obtain for the linearized form of Eq. (1) the simple diffusion equation

$$(\partial/\partial t)(\tfrac{3}{2}\Delta T_e) = (\chi_{ep}/r)(\partial/\partial r) r \partial \Delta T_e/\partial r . \quad (2)$$

The terms involving gradients of n_e and χ_{ep} have been neglected because we assume $\partial \ln \Delta T_e/\partial r \ll \partial \ln \Delta T_e/\partial r$. Similarly, if we had retained in Eq. (1) the energy convection, Ohmic heating, radiation, and other more general effects on the electron-heat-balance equation, the other terms would not have altered Eq. (2) since the temporal and spatial gradients of the temperature perturbation are much larger than those in the equilibrium.

The internal-disruption effects are introduced through a heat-pulse boundary condition that approximates the observed signal behavior near a_D: $n_e \chi_{ep} \partial \Delta T_e/\partial r|_{r=a_D} = -\Delta Q \sum_n \delta(t - nt_0)$, where ΔQ is the electron energy density in each heat pulse, t_0 is the disruption repetition time, and for simplicity the heat pulses are assumed to be δ functions of time. Solving Eq. (2) by Laplace transform techniques, subject to the condition $\Delta T_e \to 0$ for $r \to \infty$ and the above heat pulse condition, the approximate solution for the spatial region of interest ($a_D \ll r \ll a$) is found to be

$$\Delta T_e(r, t) \simeq \frac{a_D \Delta Q}{n_e \chi_{ep}} \times \sum_{n=0}^{N} \frac{\exp\{-3r^2/[8\chi_{ep}(t - nt_0)]\}}{t - nt_0}, \quad (3)$$

where $N \equiv [t/t_0]$, the largest integer less than t/t_0. For a single isolated pulse ($t_0 \gg 3r^2/8\chi_{ep}$) we have

$$\Delta T_e \simeq \tfrac{8}{3}(a_D \Delta Q/n_e r^2)(t_p/t)\exp(-t_p/t),$$
$$t_p \equiv \tfrac{3}{8} r^2/\chi_{ep}. \quad (4)$$

The important points to note about this heat-diffusion solution are (1) the peak of ΔT_e occurs at $t = t_p$, which is proportional to r^2 and inversely proportional to χ_{ep}; (2) at a given r, $\Delta T_e(t)$ increases smoothly to its peak in a time t_p and then decays roughly as t_p/t thereafter; (3) the maxima of $\Delta T_e(t)$ vary inversely with r^2—a manifestation of energy conservation in the cylindrical expansion of the heat pulse.

Before making comparisons with experiment, there are additional effects we must consider. First, since t_p is often a significant fraction of the pulse repetition time t_0, we consider $t \gg t_0$ and take account of the summation in Eq. (3). Second, what is measured is the change in the soft-x-ray intensity (ΔI) and not simply ΔT_e. However, as long as $\Delta T_e \ll T_e^2/E_c$, where E_c is the low-energy cutoff of the detectors, ΔI is the proportional to ΔT_e. Finally, we take account of the fact that the signals from the detector array are put through a 100-Hz high-pass filter before display, by multiplying the Laplace transform of ΔT_e by the transform of the filter function and using the convolution theorem to perform the inverse transform.

The experimental data are compared with the diffusive model in Fig. 2. The first point, demonstrated in Figs. 2(a) and 2(b), is that t_p agrees with the predicted asymptotic r^2 dependence.

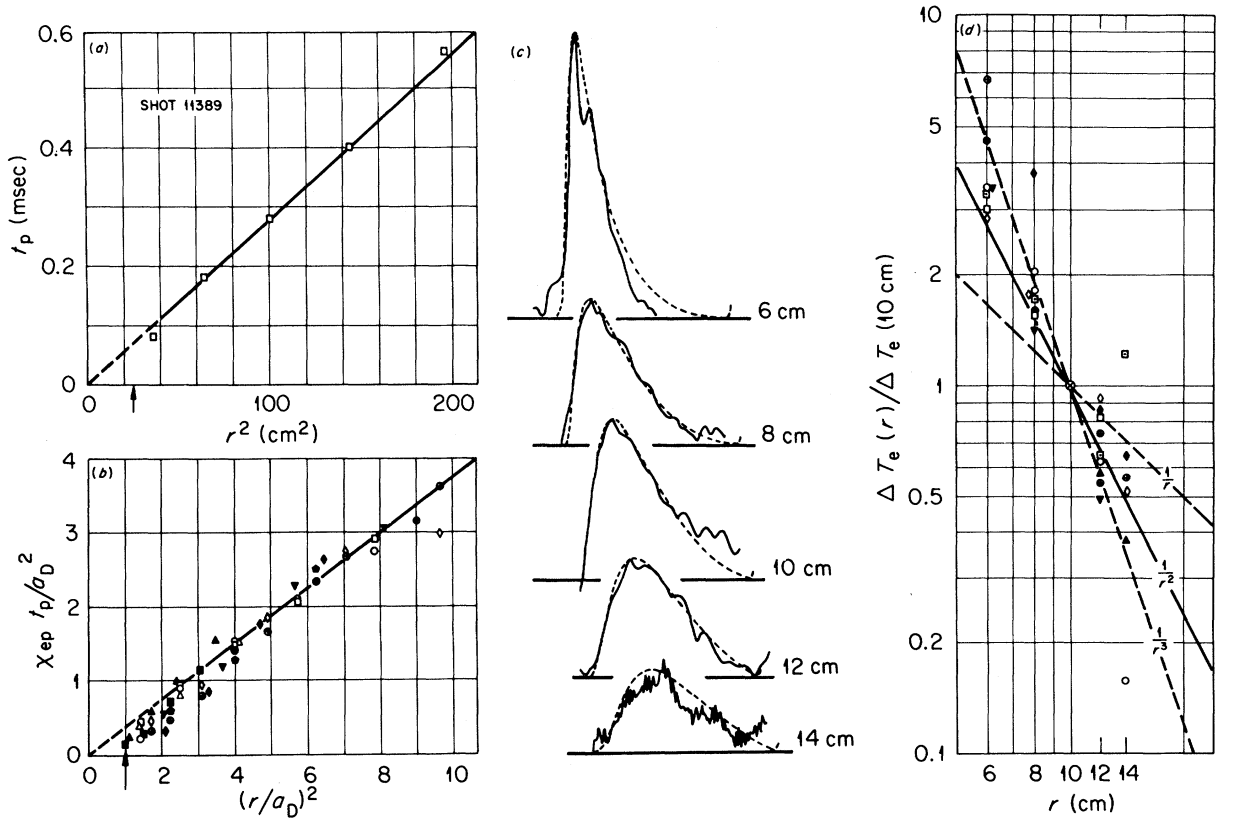

FIG. 2. Comparison of data with the diffusive model: (a) Peak arrival time vs radial position. The slope of the asymptote is $3/(8\chi_{ep})$ and thus gives a measurement of χ_{ep}. (b) t_p vs r^2 in normalized units for a representative set of discharges. Each symbol corresponds to one discharge, for which χ_{ep} has been obtained from a plot such as (a). Solid symbols are discharges with neutral-beam injection, and open symbols are for no injection. (c) Graphical reconstruction of one set of pulses (third from left in Fig. 1, shot 11 389) compared with normalized computer-generated pulse shapes. (d) Maximum ΔT_e (normalized) inferred from x-ray signal level as a function of radius.

Second, the pulse shapes follow calculated curves that include the effects of observed repetition rates and filtering [see Fig. 2(c)]. Finally, Fig. 2(d) shows that the maximum ΔT_e decreases roughly as $1/r^2$. Thus, within the limits of statistical scatter inherent in these measurements, the data show reasonable agreement with the heat-conduction model. It should be noted that due to the general irreproducibility of discharges with highly visible sawteeth,[2] approximate profiles must be used when converting the signal, ΔI, to temperature values, ΔT_e, for measurements such as the energy conservation of Fig. 2(d).

Alternative models for the pulse behavior have been considered, but no satisfactory ones found. Wave propagation cannot account for the smooth leading edge of the pulse, and would require $\max(\Delta T_e)$ to decrease as $r^{-1/2}$, instead of the observed sharper falloff. The data also do not fit with a ballistic or macroscopic plasma-flow model since in these cases the temperature pulses should simply propagate out through the plasma, essentially unchanged. *Thus, we conclude that the heat pulses produced by internal disruptions propagate out through the middle (confinement) region of ORMAK by a diffusive process, at least on length scales longer than the spatial resolution of the detector array, which is about 2 cm.*

Next, we compare the rate of this process with the gross electron energy transport. Since t_p is found to be roughly dependent on r^2 [Figs. 2(a) and 2(b)], the inferred heat-conduction coefficient χ_{ep} appears to be reasonably constant over the region observed. For comparison purposes, if we assume that electron heat conduction with coefficient $\chi_e(T_e)$ is the dominant heat-loss term in ORMAK and that the disruptive and edge layers are thin (a_D, $|a-a_0| \ll a$) then

$$\tau_{E_e} \simeq a^2/4\chi_e, \tag{5}$$

where τ_{E_e} is the electron energy containment time obtained by the usual method of dividing the

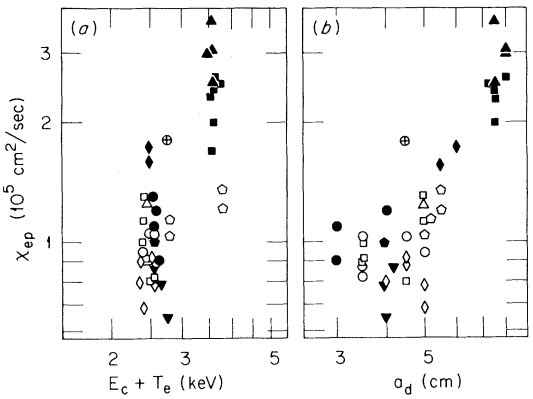

FIG. 3. Experimentally observed relationships between χ_{ep} and (a) the electron energy parameter $E_c + T_e$ (described in the text); (b) the internal disruption radius a_D.

stored energy by the power input (Ohmic, plus the fraction of injection power transferred to the electrons, minus the power to the ions). Comparisons of χ_{ep} determined from heat-pulse propagation with χ_e determined from Eq. (5) ($\sim 2\times10^4$ cm^2/sec) shows that (1) there is little correlation between χ_{ep} and χ_e; (2) χ_{ep} *exceeds* χ_e by factors ranging from 2.5 to 15; and (3) both χ_e and χ_{ep} substantially exceed the neoclassical values[4] of $(1-10)\times10^2$ cm^2/sec for these discharges. This disagreement between χ_{ep} and χ_e in both magnitude and scaling, is significant,[5] and is surprising since one expects the heat-pulse propagation to reflect the gross plasma behavior.

We do not yet understand the reason for this disagreement, but the experimental correlations shown in Fig. 3, which were obtained from a random collection of discharges, suggest possible hypotheses. First, the detectors see only photons of energies above E_c, and the dominant contribution to the detected signal comes from electrons of energy $E_c + T_e$, the abcissa in Fig. 3(a). These data suggest that the conduction coefficient associated with the pulse depends upon what electron energies are observed, and hence that the electron distribution may not be Maxwellian in the energy range of interest. The internal disruption process could produce a bi-Maxwellian initial distribution since it has the effect of mixing hot and cold components at the disruption radius. However, the time scale of interest (0.1 msec$< t_p <$ 1 msec) appears longer than the energy relaxation time at these energies [$\tau_{ee}(E_c)/2 \sim 30-50$ μsec]. Thus, Fig. 3(a) seems to suggest a faster transfer of heat at higher electron energies, but theoretically the more rapid time scale for thermalization should render such an effect small and hence unobservable.

Alternatively, Fig. 3(b) indicates a possible correlation between χ_{ep} and a_D, the disruption radius. Empirically, the size of a_D is related to the strength of the internal disruption, so the suggestion here is that the pulse propagation is significantly affected by the driving force of the sawteeth—a feature not included in our model. A problem with this interpretation is that the pulses are observed after the disruption phase has ceased and so it is not clear that the sawtooth transport mechanism would still be operating.

In conclusion, the electron temperature perturbations produced by internal disruptions are found to have a clearly diffusive space-time evolution. This heat conduction, however, is not related in a straightforward way to the transport determining the gross confinement of the device. Preliminary indications suggest that either this is a feature of observing only high-energy electrons, or that the pulse transport is influenced by the internal disruption mechanism itself.

The authors are particularly grateful to J. L. Dunlap and J. H. Harris for their close experimental participation, to the TFR group (Fontenay-aux-Roses, France) for constructive communications on related work, and to J. L. Whitson for the numerical computations. They are also grateful to R. G. Bateman, L. A. Berry, J. F. Clarke, R. A. Dandl, H. C. Howe, M. Murakami, O. P. Manley, J. A. Rome, S. Von Goeler, and K. T. Tsang for many useful discussions of this work.

*Research sponsored by U. S. Energy Research and Development Administration under contract with Union Carbide Corporation.

[1]S. Von Goeler, W. Stodiek, and N. Sauthoff, Phys. Rev. Lett. 33, 1201 (1974).

[2]J. L. Dunlap, G. L. Jahns, and J. H. Harris, Bull. Am. Phys. Soc. 20, 1255 (1975); J. L. Dunlap *et al.*, to be published.

[3]R. Dei-Cas, in Proceedings of the Sixth International Conference on Plasma Physics and Controlled Nuclear Fusion Research, Berchtesgaden, West Germany, 6–13 October 1976 (to be published), Paper No. CN-351A8; J. Hosea and V. Arunasalam, Bull. Am. Phys. Soc. 21, 1159 (1976).

[4]F. L. Hinton and M. N. Rosenbluth, Phys. Fluids 16, 836 (1973), and references cited therein.

[5]Transport simulation calculations using a coefficient as large as χ_{ep} result in an electron temperature much lower than experimentally observed (H. C. Howe, private communication).

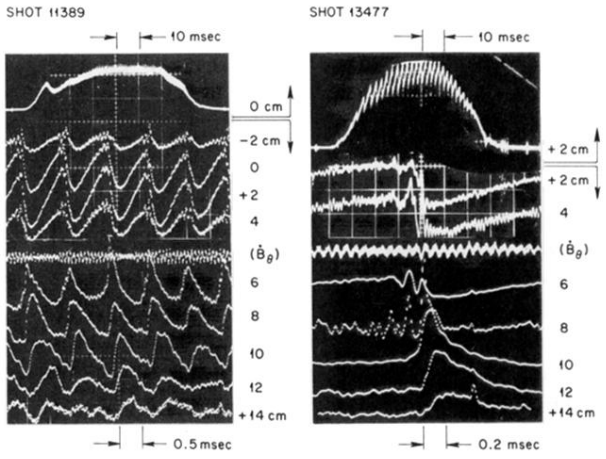

FIG. 1. Composite oscillograms of soft-x-ray signals for two discharges. For both cases, the top trace gives the signal from one detector over the full time of the discharge; the rest of the signals are on an expanded timescale starting at 45 msec, which falls in the middle of the full-time trace. Amplification factors are different for purposes of display. The temporal variation in the signal (sharp fall inside, sharp rise outside) shows that a_D is $\simeq 5$ cm for shot 11 389 and $\simeq 8$ cm for shot 13 477. The signals labeled $\dot{B}_\theta$ are poloidal magnetic field fluctuations from pickup loops.